Platelets are mediators and interventional targets of non-alcoholic steatohepatitis and liver cancer

Mohsen Malehmir[1], Dominik Pfister[2,*], Donato Inverso[3,*], Elena Kotsiliti[2,4,*], Valentina Leone[2,5,*], Dominik Rath[6], Monika Julia Wolf[1], Marc Eamonn Healy[1], Daniel Dauch[7,8], Carsten Deppermann[9], Julia Volz[9], David Stegner[9], Patrick Helbling[10], César Nombela-Arrieta[10], Anahita Rafiei[10], Martina Steurer[7,8], Marcel Rall[6], Florian Baku[6], Caroline L. Wilson[11], Tracy O`Connor[2], Ana Teijeiro[12], Malte Bongers[13], Mike Notohamiprodjo[13], Josep M. Llovet[14,15], Roser Pinyol[14,15], Tobias Geisler[6], Hellmut Augustin[3,16], Patricia F. Lalor[17], Jerry Ware[18], Percy A. Knolle[19], Nabil Djouder[12], Kristian Unger[5], Lars Zender[7,8,20], Bernhard Nieswandt[9], Meinrad Gawaz[6], Achim Weber[1,**] & Mathias Heikenwalder[2,3,**]

1. Department of Pathology and Molecular Pathology, University and University Hospital Zurich, Zurich, Switzerland
2. Division of Chronic Inflammation and Cancer, German Cancer Research Center Heidelberg (DKFZ), Heidelberg, Im Neuenheimer Feld 280, 69120 Heidelberg, Germany
3. Division of Vascular Oncology and Metastasis, German Cancer Research Center Heidelberg (DKFZ-ZMBH Alliance), Im Neuenheimer Feld 280, 69120 Heidelberg, Germany
4. Institute for Virology, Technische Universität München/Helmholtz Zentrum München, Munich, Germany
5. Research Unit of Radiation Cytogenetics, Helmholtz Zentrum München, Neuherberg Germany
6. Department of Cardiology and Circulatory Diseases, Internal Medicine Clinic III, Eberhard Karls University Tübingen, Tübingen, Germany
7. Department of Internal Medicine VIII, University Hospital Tübingen, 72076 Tübingen, Germany
8. Department of Physiology I, Institute of Physiology, Eberhard Karls University Tübingen, 72076 Tübingen, Germany
9. Institute of Experimental Biomedicine, University Hospital and Rudolf Virchow Center, University of Würzburg, Würzburg, Germany
10. Hematology, University Hospital and University of Zurich, Zurich, Switzerland
11. Institute of Cellular Medicine, Faculty of Medical Sciences, 4th Floor, William Leech Building, Newcastle University, Framlington Place, Newcastle upon Tyne NE2 4HH, UK
12. Cancer Cell Biology Programme, Growth Factors, Nutrients and Cancer Group, Centro Nacional de Investigaciones Oncológicas (CNIO), Madrid 28029, Spain

13. Department of Diagnostic and Interventional Radiology, Eberhard Karls University Tübingen, Tübingen, Germany
14. Mount Sinai Liver Cancer Program (Divisions of Liver Diseases, Department of Medicine, Department of Pathology, Recanati Miller Transplantation Institute), Tisch Cancer Institute, Icahn School of Medicine at Mount Sinai, New York, USA
15. Liver Cancer Translational research laboratory, BCLC Group, IDIBAPS, Liver Unit, Hospital Clinic, University of Barcelona, Barcelona, Catalonia, Spain; Institució Catalana de Recerca i Estudis Avançats, Barcelona, Catalonia, Spain
16. Department of Vascular Biology and Tumor Angiogenesis, Medical Faculty Mannheim (CBTM), Heidelberg University, Mannheim, Germany.
17. Centre for Liver Research and National Institute for Health Research (NIHR) Birmingham Liver Biomedical Research Unit, Birmingham B152TT, United Kingdom
18. Department of Physiology and Biophysics, University of Arkansas for Medical Sciences, 4301 West Markham Street, Little Rock, Arkansass 72205, USA
19. Institute of Molecular Immunology and Experimental Oncology, Technical University of Munich, Ismaningerstraße 22, 81675 Munich, Germany
20. Translational Gastrointestinal Oncology Group, German Consortium for Translational Cancer Research (DKTK), German Cancer Research Center (DKFZ), 69120 Heidelberg, Germany.

* contributed equally

** share last and corresponding authorship

SUMMARY

Nonalcoholic fatty liver disease (NAFLD) ranges from steatosis to nonalcoholic steatohepatitis (NASH), which may progress to cirrhosis and hepatocellular carcinoma (HCC). In a murine model we have previously recapitulated human NAFLD/NASH pathophysiology demonstrating that $CD8^+$ T- and NKT-cells interact with hepatocytes to induce NASH and NASH-to-HCC transition. Here, we show that platelet numbers and their activation-state are increased in murine and human NASH. Antiplatelet therapy (APT) with aspirin/clopidogrel or ticagrelor prevented NASH-to-HCC transition. APT reduced intrahepatic platelet-accumulation, platelet-liver endothelium and platelet-immune cell interaction, thereby limiting hepatic immune-cell trafficking. Consequently, liver damage, cytokine release and macro-vesicular steatosis declined, resulting in protection against NAFLD and NASH-to-HCC transition. In line, NAFLD-patients revealed reduced liver volume, liver fat content and liver enzymes after 6 months of APT. Performing genetic and functional analyses, we identified glycoprotein (GP) GPIIb/IIa, GPVI, von-Willebrand-factor and P-selectin to be dispensable, whereas GPIbα and α-granules proved as critical drivers of NASH.

INTRODUCTION

Hepatocellular carcinoma (HCC) is the third most common cause of cancer-related death and is the fastest rising cancer in the United States with similar trends in Europe[1-3]. Nonalcoholic fatty liver disease (NAFLD) has become the most common chronic liver disease in high-income countries, affecting up to one-third of adults as well as a substantial proportion of children[4] and is on trajectory to become the most common indication for liver transplantation in the United States[5,6]. NAFLD comprises a disease spectrum ranging from simple steatosis (non-alcoholic fatty liver (NAFL)) to nonalcoholic steatohepatitis (NASH) which may progress to cirrhosis and ultimately HCC[7-9]. Major risk factors associated with NASH include metabolic syndrome, abdominal obesity, insulin resistance, glucose intolerance or type 2 diabetes mellitus and dyslipidaemia[10-14].

We previously developed a pre-clinical model which recapitulates the features of human metabolic syndrome, hepatic inflammation, NASH and NASH-induced HCC[15]. We showed that intrahepatic influx of metabolically activated $CD8^+$ T- and NKT-cells triggers metabolic reprogramming of hepatocytes, NASH and HCC development through cytokine-mediated cross talk with hepatocytes. However, the mechanisms underlying immune cell recruitment to the liver in the context of NASH and its consequences for NASH-to-HCC transition have remained unclear.

Platelets, produced by megakaryocytes in the bone marrow, play a fundamental role in hemostasis[16], but are also crucial for pathophysiological conditions like thrombosis[17], atherosclerosis[18], metastasis[19] and stroke[20]. In addition, a growing body of evidence highlights platelets as active players in liver disease and inflammation[21-24]. Notably, it has been reported that activated platelets contribute to cytotoxic T lymphocyte (CTL)-mediated liver damage[25]. Moreover, blocking platelet

activation and aggregation by Aspirin-Clopidogrel (Asp-Clo) abrogates hepatic T cell influx, subsequent liver damage and tumorigenesis without affecting peripheral T cell function[26,27].

NASH and HCC incidence are increasing, highlighting a significant unmet need for efficacious, low risk therapies against NASH and NASH-to-HCC transition. At the same time, although several drugs are in phase 2 and 3 development[28,29], currently no approved pharmacological therapies are available which prevent NASH or related pathologies including HCC. The role of platelets in NASH and related HCC development is unknown. Thus, we aimed to investigate whether antiplatelet therapy (APT) might interfere with NASH and NASH-induced HCC development.

RESULTS

Hepatic accumulation of activated platelets is observed in NASH

To test whether platelets contribute to NASH development, we investigated the number and distribution of platelets in the liver of C57Bl/6 mice fed a choline-deficient high fat diet (CD-HFD). Quantification of $CD42b^+$ (GPIb) platelets demonstrated a significantly increased number in livers of CD-HFD-fed mice compared to age-matched normal diet (ND)-fed controls (**Fig. 1a**). Platelet aggregation (number, aggregate size) was strongly increased in livers of CD-HFD-fed mice (**Fig. 1b**). Platelet counts in peripheral blood remained normal (**Supplementary Fig. 1a**). Whereas fibrinogen levels and prothrombin time (PT) remained unchanged, activated partial thromboplastin time (aPTT) was significantly reduced in CD-HFD-fed mice (**Supplementary Fig. 1b-d**). *Ex vivo* analysis of circulating platelets revealed no significant differences in activation/aggregation responses in CD-HFD-fed mice compared to ND-fed mice, as measured by αIIbβ3 integrin activation and P-selectin exposure upon stimulation with different agonists (**Supplementary Fig. 1e**). We next analyzed another murine NASH model, an inducible knock-in expressing the human unconventional prefoldin RPB5 interactor (URI) in hepatocytes (hURI-tetOFFhep)[30]. hURI-tetOFFhep mice showed a significant increase in intrahepatic platelets compared to non-induced controls (**Fig. 1c**). These data identify abnormal intrahepatic platelet aggregation as a common pathological feature of murine NASH.

Human NAFLD/NASH patients displayed a significant increase in $CD61^+$ platelets in the liver compared to healthy controls (**Fig. 1d; Table S1**), supporting the hypothesis that NASH is accompanied by increased intra-hepatic accumulation of activated platelets.

Asp-Clo treatment constitutes an APT currently used for blocking platelet activation/aggregation in several diseases (e.g. coronary stent thrombosis[31]). We first addressed whether CD-HFD-fed mice would respond to APT. Compared to untreated mice on CD-HFD, Asp-Clo-treated mice on CD-HFD displayed significantly reduced intrahepatic platelet numbers (**Fig. 1e**). Moreover, Asp-Clo treatment significantly reduced intrahepatic platelet aggregation compared to CD-HFD-fed controls (**Supplementary Fig. 1f-h**)**.**

To investigate the effects of APT treatment on human NAFLD, serum samples from patients at high cardiovascular risk who had undergone heart catheter procedure were retrospectively analysed. Patients at risk for NAFLD (n=147) had several cardiovascular risk factors including obesity, arterial hypertension, hyperlipidemia, smoking and/or diabetes mellitus type II, increased LDL, vLDL and serum cholesterol levels compared to controls (**Supplementary Fig. 1i,j** and **Table S2**). Serum samples were obtained from each patient before and after APT (6 months). In a subgroup of patients (n=30), we performed platelet function analysis, showing that patients generally responded well to APT (**Supplementary Fig. 1k**). Although serum cholesterol, LDL and HDL levels remained unchanged in this cohort (**Supplementary Fig. 1l-n**), a significant reduction in serum alanine and aspartate transaminase (ALT; AST) levels following APT was observed (**Fig. 1f**).

We performed a prospective clinical trial (German Clinical Trials Register (DRKS) 587/2016BO2) with NAFLD patients (e.g. BMI>30; obesity, arterial hypertension, hyperlipidemia, diabetes mellitus type II, constantly increased LDL, vLDL and serum cholesterol levels; n=13) undergoing a heart catheter procedure and subsequent APT treatment for 6 months (**Table S3**). For control, we investigated patients left untreated (**Table S3**). NAFLD patients were monitored for 6 months after heart

catheter implantation and analyzed using serology, MRI and sonography for several parameters. APT-treated NAFLD patients displayed reduced serum liver enzyme levels, indicative for live damage (ALT, AST) and a significant reduction in liver volume and liver fat mass compared to values upon study inclusion (**Fig. 1g,h** and **Supplementary Fig. 1o**). Collectively, these data suggest that APT has beneficial effects in both murine and human NAFLD.

Antiplatelet treatment with Asp-Clo attenuates NASH and NASH-associated conditions

We next determined whether Asp-Clo treatment affects conditions associated with NASH and NASH-to-HCC transition in mice. C57Bl/6 mice were given ND, CD-HFD or CD-HFD/Asp-Clo and analyzed at 6 and 12 months of age. Weight gain over time was significantly higher in CD-HFD and CD-HFD/Asp-Clo-fed mice compared to ND-fed controls. No significant difference in weight gain or white adipose tissue mass was found between mice on CD-HFD or CD-HFD/Asp-Clo (**Fig. 2a** and **data not shown**). In contrast, liver damage (ALT; AST), liver/body weight ratio, platelet number and aggregation were significantly reduced in mice on CD-HFD/Asp-Clo at 6 and 12 months of age (**Fig. 2b** and **Supplementary Fig. 1f, 2a,b**). Asp-Clo treatment significantly improved glucose tolerance compared to untreated CD-HFD-fed mice at 6 months of age (**Fig. 2c**). Analysis of ND, CD-HFD and CD-HFD/Asp-Clo-fed mice revealed a significant reduction of liver triglycerides in CD-HFD/Asp-Clo-treated mice at 6 and 12 months of age (**Fig. 2d**). Similarly, serum cholesterol, LDL and HDL declined in CD-HFD/Asp-Clo mice to levels similar to ND-fed C57Bl/6 mice at this age (**Fig. 2e** and **Supplementary Fig. 2c,d**). This suggests that Asp-Clo effectively reduced dyslipidaemia and liver/body weight ratio, but not total body weight. To

evaluate activation responses in platelets, P-selectin as a marker of α-granule release and integrin αIIbβ3 activation were analyzed by flow cytometry. In Asp-Clo-treated CD-HFD mice, circulating platelets showed markedly reduced integrin αIIbβ3 activation and P-selectin exposure compared with ND and CD-HFD platelets in response to all tested agonists (**Supplementary Fig. 2e**), suggesting that Asp-Clo treatment effectively reduced local, intrahepatic platelet activation. Of note, levels of major platelet surface glycoproteins were indistinguishable between the different groups (**Supplementary Fig. 2f**). Several genes involved in lipid metabolism and β-oxidation are dysregulated during NASH development[15]. Notably, Asp-Clo treatment prevented downregulation of these metabolic genes in CD-HFD-fed mice (**Fig. 2f**).

MRI-analysis revealed subcutaneous/abdominal fat accumulation in CD-HFD and CD-HFD/Asp-Clo treated mice, but not in ND-fed controls. However, liver steatosis was ameliorated or even prevented by Asp-Clo treatment in CD-HFD mice (**Fig. 2g**). This was in line with reduced intrahepatic triglyceride deposition upon Asp-Clo treatment (**Fig. 2d**). CD-HFD-fed mice displayed histopathological features of NASH such as steatosis, ballooning of hepatocytes, Mallory-Denk body formation, lobular inflammation including satellitosis, occasional minimal fibrosis) (**Fig. 2h** and **data not shown**). Similar to steatosis analyzed by MRI, pathological features of NASH were reduced or abolished by Asp-Clo treatment (**Fig. 2h-i**). We concluded that Asp-Clo treatment effectively reduces or inhibits NASH development.

Asp-Clo abrogates intrahepatic immune-cell infiltration and inhibits NASH-induced HCC

In addition to the hepatic infiltration of $CD3^+CD8^+$T cells, increased numbers of $MHCII^+$ myeloid cells and Ly-$6G^+$ granulocytes were reported in CD-HFD-fed C57Bl/6 mice, recapitulating key features of steatohepatitis in NASH patients[15]. Immune-cell infiltrates were minimal in CD-HFD/Asp-Clo treated C57Bl/6 mice at 6 and 12 months of age (**Fig. 3a**). Flow cytometry also demonstrated a strong reduction in total number, effector differentiation ($CD8^+CD62L^-CD44^+CD69^+$) and proportion of $CD8^+CD4^-$ and NKT-cells (**Fig. 3b**). Several inflammatory signaling pathways activated under CD-HFD, e.g. canonical NF-κb activation (pp65, p38, pStat3, pERK), were partially or completely reduced by Asp-Clo treatment (**Fig. 3c** and **Supplementary Fig. 3a**). Altogether, Asp-Clo treatment prevented key features of NASH and dampened pathways that support hepatocarcinogenesis[32,33].

Next, we studied the effect of Asp-Clo treatment on CD-HFD-induced HCC development[15]. Mice were sacrificed at 12 months of age and livers analyzed macro- and microscopically. CD-HFD-fed mice showed enlarged, pale yellow livers indicative of steatosis. 13 out of 51 CD-HFD-fed mice displayed macroscopically visible tumors (incidence ~25%) (**Fig. 3d,e**). In contrast, all CD-HFD/Asp-Clo treated mice lacked macroscopically visible liver tumors. Histology (H/E) and IHC including collagen IV, glutamine synthetase (GS) and serum golgi protein 73 (GP73) corroborated that CD-HFD-fed mice displayed tumors, the progressed ones of which represented HCC (**Fig. 3f** and **Supplementary Fig. 3b**). In addition, microscopic analysis showed no evidence of HCC in mice treated with CD-HFD/Asp-Clo. Of note, CD-HFD-fed mice, treated with a low dose of Asp-Clo (according to the initial body weight and not adjusted to weight gain), also developed significantly less HCC compared to untreated CD-HFD-fed mice (**Supplementary Fig. 3c**). Therefore, the dose of Asp-Clo (adjusted to body weight) is critical to fully prevent HCC development.

Beneficial effects of Asp treatment are also thought to emanate from the decreased production of prostaglandins and thromboxane[34]. Our data did not exclude non-platelet specific effects of Asp. Indeed, a strong reduction in COX2 protein expression was found in liver homogenates from CD-HFD/Asp-Clo mice when compared to ND or CD-HFD controls (**Fig. 3c**). To investigate this further, we used another non-steroidal anti-inflammatory drug (NSAID) COX1/2 inhibitor: sulindac. CD-HFD/sulindac-treated mice exhibit obesity, no significant changes in liver/body weight ratio, severe steatosis, NASH and NASH-associated conditions comparable to CD-HFD treated mice (**Supplementary Fig. 4a-j**). Thus, Asp/Clo mediated effects on NASH are COX-independent.

Ticagrelor prevents NASH and HCC development

To corroborate our hypothesis that inhibiting platelet activation/aggregation ameliorates NASH and NASH-induced HCC, CD-HFD-fed mice were treated with ticagrelor (CD-HFD/ticagrelor), a direct and reversible P2Y12 antagonist[35,36], currently in phase IV clinical trials for coronary artery disease (CAD; https://www.clinicaltrials.gov). A significant weight gain in CD-HFD- and CD-HFD/ticagrelor-treated mice was observed at 6 and 12 months of age, compared to ND-fed controls (**Fig. 4a**). However, ticagrelor treatment significantly reduced liver damage observed under CD-HFD (**Fig. 4b**). Liver/body weight ratio was not significantly affected in mice on CD-HFD/ticagrelor compared to CD-HFD controls (**Supplementary Fig. 5a**). Although serum cholesterol levels were significantly reduced we could only find a non-significant reduction of liver triglyceride levels (**Fig. 4c,d**). Notably, glucose intolerance was not ameliorated with ticagrelor treatment (**Supplementary Fig. 5b**). Moreover, downregulation of several genes involved in

lipid metabolism/β-oxidation (e.g. Cpt1, Acox3, Lpl) was prevented (**Supplementary Fig. 5c**). Strikingly, histological analyses demonstrated that CD-HFD-induced features of NASH were abolished upon ticagrelor treatment (**Fig. 4e**). This was corroborated by a significant reduction of lipid droplets and absent or strongly reduced macro-vesicular steatosis (**Fig. 4f**). Flow cytometry demonstrated statistically significant reduction in total number, activation and proportion of $CD4^+CD8^+$, $CD8^+CD62L^-D44^+CD69^+$ and $CD3^+NK1.1^+$ cells (**Fig. 4g-h**). This was corroborated by IHC revealing a reduction in T-cell infiltration, recruitment of $Ly6G^+$ granulocytes and macrophages to the liver (**Fig. 4i** and **Supplementary Fig. 5d-e**). Next, we investigated whether ticagrelor treatment would also diminish or block CD-HFD-triggered HCC. Mice fed with ND, CD-HFD or CD-HFD/ticagrelor (12 months of age) were analyzed macroscopically and microscopically for liver cancer development. In contrast to C57Bl/6 mice on CD-HFD, only a single non-HCC liver nodule was detectable in 29 CD-HFD/ticagrelor-treated mice (**Fig. 4j,k** and **Supplementary Figure 5f**). Collectively, these results demonstrated that ticagrelor treatment prevents NASH and HCC development.

Platelet-derived GPIbα and α-granules are required to induce NASH and NASH-associated conditions

To study the mechanisms by which platelets contribute to NASH in more detail, we analysed the involvement of major adhesion receptors. The platelet-specific glycoprotein (GP)Ib-V-IX complex constitutes a multifunctional adhesion molecule receptor. It is exclusively expressed on platelets and megakaryocytes with the GPIbα subunit harboring the binding sites for its major ligands, most notably von-Willebrand-factor (vWF), which is critical for platelet adhesion and plug formation under high

shear flow conditions[37,38]. In addition, GPIbα is increasingly recognized as a central orchestrator of thrombo-inflammatory processes[39], in part by interacting with receptors on immune cells (Mac1) and endothelial cells (P-selectin). We hypothesized that GPIbα mediates platelet-trafficking in inflamed livers during NASH, contributing to efficient immune cell-trafficking to the liver. To test this hypothesis, we first blocked the major ligand binding domain of GPIbα in 5-6 months old CD-HFD-fed C57Bl/6 mice using Fab fragments of the anti-GPIbα antibody, pop/B[39] for 4 weeks. Strikingly, anti-GPIbα treatment significantly reduced platelet accumulation in the liver (**Fig. 5a**).

Next, we took advantage of transgenic mice expressing an IL-4rα/GPIbα fusion-protein in a GP1bα$^{-/-}$ background (a model for Bernard-Soulier syndrome[40]), in which the ligand binding ectodomain of GPIbα is replaced by the α-subunit of the human IL-4 receptor (hIL4rα/GP1bα-Tg mice[40]). This model enabled us to specifically dissect the role of functional GPIbα in NASH *in vivo*. C57Bl/6 control and hIL4rα/GP1bα-Tg mice were fed with CD-HFD and monitored over 6 months. CD-HFD/hIL4rα/GP1bα-Tg mice gained weight similarly to C57Bl/6 mice on CD-HFD (**Fig. 5b**). A significant reduction in serum ALT and AST levels was observed in CD-HFD/hIL4rα/GP1bα-Tg mice (**Fig. 5c** and **Supplementary Fig. 6a**), accompanied by reduced liver triglycerides, serum cholesterol, serum LDL and HDL (**Fig. 5d-g**). Similarly, dysregulated mRNA expression of lipid metabolism-related genes in CD-HFD-fed C57BL/6 livers was prevented in livers of CD-HFD/hIL4rα/GP1bα-Tg mice (**Fig. 5h**). Strikingly, compared to C57Bl/6 mice on CD-HFD, CD-HFD/hIL4rα/GP1bα-Tg mice lacked histological features of NASH, paralleled by a reduction of lipid accumulation and absence of macrovesicular steatosis analyzed by H/E and Sudan red staining (**Fig. 5i,j**). Concomitant with the reduction of steatosis and NASH, we observed a strong and significant reduction in intra-hepatic CD8^{+} T- and NKT-cells

(**Supplementary Fig. 6b**). In addition, decreased neutrophil accumulation and macrophage influx/activation were observed (**Supplementary Fig. 6c**). These data suggest that anti-GPIbα treatment reduces hepatic platelet number/aggregation and that lack of functional GPIbα protects against liver damage, NASH and NASH-associated conditions.

Several studies have shown the importance of vWF interaction with its receptor GPIb-IX-V for initiating platelet adhesion and aggregation[38,41,42]. To test whether vWF was required for GPIbα to promote the development of NASH, we used vWF knockout mice (*vWF*$^{-/-}$) and monitored them for 6 months under CD-HFD. CD-HFD-fed *vWF*$^{-/-}$ mice showed severe steatosis, NASH and NASH-associated conditions, even more severe than CD-HFD-fed C57Bl/6 mice (**Supplementary Fig. 7a-i**). These results suggest that GPIbα-mediated NASH development is independent of vWF.

Next, we investigated whether platelet aggregation is a critical step in the development of NASH. To this end, we assessed mice lacking the GPIIb subunit of the platelet fibrinogen receptor, GPIIb/IIIa (integrin $\alpha 2\beta 3$; *Itga2b*$^{-/-}$ mice). CD-HFD-fed *Itg2b*$^{-/-}$ mice display a similar degree of weight gain, liver/body weight ratio and liver damage, compared to CD-HFD-fed C57Bl/6 mice (**Fig. 5k-m**). Moreover, CD-HFD-fed *Itga2b*$^{-/-}$ mice displayed liver trigylcerides, serum cholesterol and equally impaired glucose tolerance as CD-HFD-fed C57Bl/6 mice (**Fig. 5n,o** and **Supplementary Fig. 8a**). In line, dysregulated mRNA expression of genes involved in lipid metabolism/β-oxidation, NASH and NASH-associated conditions remained mostly unchanged (**Fig. 5p** and **Supplementary Fig. 8b,c**).

Moreover, we analyzed CD-HFD-fed mice that lack the activating platelet collagen receptor glycoprotein VI (GPVI)[43]. CD-HFD-fed *Gp6*$^{-/-}$ mice displayed a similar

degree of weight gain, liver/body weight ratio and not significantly altered liver damage, as compared with CD-HFD-fed C57Bl/6 mice (**Supplementary Fig. 9a-c**). Moreover, CD-HFD-fed *Gp6*$^{-/-}$ mice showed similarly increased liver trigylcerides, significantly raised serum cholesterol and likewise impaired glucose tolerance, as CD-HFD-fed C57Bl/6 mice (**Supplementary Fig. 9d-f**). In line, dysregulated mRNA expression of genes involved in lipid metabolism/β-oxidation, NASH and NASH associated conditions remained (**Supplementary Fig. 9g**). Finally, *Gp6*$^{-/-}$ mice displayed significantly more macro-vesicular steatosis and histopathology of NASH (**Supplementary Fig. 9h,i**). These data underline that platelet activation and adhesion are central to NASH development. In contrast, platelet aggregation - although observed - is functionally irrelevant for NASH pathology.

Platelets store a plethora of bioactive factors in their intracellular granules and release them in response to cellular activation. In the course of thrombo-inflammatory reactions, the mostly proteinous components of α–granules have been shown to be essential for immune cell recruitment and tissue damage[44]. To study a possible involvement of α-granule release to the development of NASH, we took advantage of Nbeal2 knock-out mice (*Nbeal2*$^{-/-}$) which lack α-granules in their platelets. These mice recapitulate the hallmarks of the human Gray Platelet Syndrome (GPS), a rare bleeding disorder. Thus, they are protected from thrombosis and thrombo-inflammatory tissue damage[45-47]. We fed *Nbeal2*$^{-/-}$ mice with CD-HFD over 6 months. CD-HFD-fed *Nbeal2*$^{-/-}$ gained weight similarly to their C57Bl/6 counterparts, both being significantly heavier than C57Bl/6 ND-fed mice (**Supplementary Fig. 10a**). Strikingly, a strong reduction in serum ALT and AST levels was found in CD-HFD-fed *Nbeal2*$^{-/-}$ mice compared to CD-HFD-fed C57Bl/6 mice (**Supplementary Fig. 10b**). Moreover, a trend in reduction of liver/body weight ratio in CD-HFD-fed *Nbeal2*$^{-/-}$ was

found, when compared to CD-HFD-fed controls (**Supplementary Fig. 10c**). This was paralleled by a significant decrease in liver triglycerides and serum cholesterol in CD-HFD-fed *Nbeal2*$^{-/-}$ mice when compared to CD-HFD-fed controls (**Supplementary Fig. 10d,e**). A significant improvement in glucose tolerance was found in *Nbeal2*$^{-/-}$ mice when compared to CD-HFD C57Bl/6 mice (**Supplementary Fig. 10f**). Deregulation of lipid metabolism genes in CD-HFD C57Bl/6 livers was partially prevented in livers of CD-HFD/*Nbeal2*$^{-/-}$ mice (**Supplementary Fig. 10g**). In contrast to C57Bl/6, *Nbeal2*$^{-/-}$ mice on CD-HFD lacked histological features of steatosis or NASH (**Supplementary Fig. 10h**). Reduction or suppression of NASH in *Nbeal2*$^{-/-}$ mice on CD-HFD was corroborated by significant diminution in lipid content and strong reduction in macrovesicular steatosis (**Supplementary Fig. 10i**). In line, a decrease in T-cell infiltration, neutrophil accumulation and macrophage activation was found in *Nbeal2*$^{-/-}$ mice on CD-HFD (**Supplementary Fig. 10j**). Together, these results indicated that platelet α-granule components contribute to NASH and NASH-associated conditions. Interestingly, mice lacking the α-granule residing adhesion receptor P-selectin[48] (*Selp*$^{-/-}$ mice) developed NASH and NASH-associated conditions upon CD-HFD, excluding a key role of P-selectin in this process (**Supplementary Fig. 11a-h**).

APT dampens hepatic cytokine/chemokine expression, platelet-liver endothelium and platelet-immune cell interaction

Gene-expression and signaling-pathway analyses were performed in whole liver homogenates of ND- and CD-HFD-fed C57Bl/6 mice based on RNA microarray analysis. Gene-set enrichment analyses (GESA) revealed a statistically significant enrichment for gene expression profiles involved in platelet activation, aggregation

and degranulation in CD-HFD-fed mice (**Fig. 6a, upper row** and **Supplementary Fig. 12a-c**).

Moreover, a NASH-related enrichment of genes indicative of expression of TNF-superfamily members and cytokine/chemokine production/cytokine receptor interaction was found in line with recently published studies[15,30] (**Figure 6b** and **Supplementary Figure 12d-f**). Besides, we also found significant changes in immune-cell attraction and chemotaxis (**Fig. 6a, lower row** and **Supplementary Fig. 12g,h**). Next, the effect of Asp-Clo treatment was analyzed by protein studies (multiplex ELISA) (**Fig. 6b**). A significant upregulation of several cytokines/chemokines known to attract adaptive immune cells (e.g. CXCL9, CXCL10, CCL2, CCL5 and IL15) was found in CD-HFD-fed C57Bl/6 mice (**Fig. 6b** and **Supplementary Fig. 12g,h**). Asp-Clo treatment significantly reduced the latter, some of which are also released from activated platelets (e.g. CCL5, TGFβ[49]).

We hypothesized that activated platelets interact with both liver sinusoidal endothelial and immune cells. We first coupled high-resolution confocal microscopy and 3D-reconstruction of liver sinusoids to visualize and quantify the interaction of platelets with the liver endothelium and with immune cells at single cell level (**Fig. 6** and **Supplementary 13**). Livers of CD-HFD-fed C57Bl/6 mice exhibited strongly increased platelet-liver endothelium interactions compared to ND-fed controls, which was significantly reduced by Asp-Clo or ticagrelor treatment (**Fig. 6c,d**). Similarly, platelet aggregate size was increased in NASH livers, likely reflecting a higher activation state of the cells. In contrast, Asp-Clo or ticagrelor treatment significantly reduced the size of intrahepatic platelet aggregates, reflecting reduced platelet activation (**Fig. 6d**). Remarkably, platelet numbers, aggregate size, platelet area and

platelet-liver endothelium coverage were also strongly reduced in hIL4Rα/GPIbα-Tg mice on CD-HFD compared to CD-HFD-fed C57Bl/6 controls (**Fig. 6d**).

Next, we analyzed the intra-hepatic recruitment of different immune cells under ND, CD-HFD and CD-HFD/Asp-Clo. We observed a significantly higher frequency of $CD3^+$ T-cells adherent to platelet aggregates in NASH livers, which was significantly decreased by Asp-Clo treatment (**Fig. 6e**). Moreover, fluorescence intensity profile of endothelium lining and single $CD3^+$ T-cells (without platelets) indicated a stronger $CD3^+$ T-cell-liver endothelium interaction in CD-HFD- compared to ND-fed mice, which was significantly decreased by Asp-Clo treatment (**Fig. 6f** and **Supplementary Fig. 13a**). In line, platelets strongly interacted with $CD8^+$ T-cells in NASH livers but less so in livers of ND-fed controls (**Supplementary Fig. 13b**).

Although no increase in $B220^+$ B-/dendritic-cell numbers was found by FACS or IHC in NASH livers compared to controls[15] (**Fig. 3a, Supplementary Fig.13c** and **data not shown**), a significant rise in the interaction between platelets and $B220^+$ B-/dendritic cells was found. The latter was reduced by trend upon Asp-Clo treatment (**Supplementary Fig. 13c**). We also observed increased numbers of $F4/80^+$ aggregates in NASH livers, which were associated with significantly more platelet aggregates when compared to ND-fed livers (**Supplementary Fig. 13d**). This increased platelet-$F4/80^+$ Kupffer-cell interaction was reduced upon Asp-Clo treatment, without substantially changing the total numbers of $F4/80^+$ cells but rather the number of $F4/80^+$ aggregates. In contrast, an increase in $CD11b^+$ cells was observed in NASH livers compared to ND-fed mice, corroborating previously published data[15]. In addition, intrahepatic $CD11b^+$ cells displayed a significantly increased interaction with platelets under CD-HFD, which returned to ND levels under Asp-Clo treatment (**Fig. 6g**). Thus, platelet adhesion and activation, but not

aggregation, contribute to enhanced platelet-endothelial and platelet-immune-cell interaction. This finding strongly supports a role for platelets in enhancing intrahepatic influx of immune cells during NASH, thereby driving chronic liver disease, liver fatification and subsequent HCC development.

DISCUSSION

Here, we demonstrate that platelets are mediators and interventional therapeutic targets of NASH and subsequent HCC development, thus providing the rationale for a new treatment modality against a metabolic disease of major public health relevance[10,14]. Except for an improvement of life-style (e.g. weight loss, exercise), there is no approved treatment for NASH or NASH-associated diseases (e.g. liver cancer)[10,50]. Although some agents like obeticholic acid have been shown to improve histological features of NASH, data with respect to their long-term benefits are still awaited[51]. We demonstrate that APT (e.g. Asp-Clo) used for acute and long-term treatment of patients with myocardial infarction[52], as well as ticagrelor, currently in phase IV clinical trial for CAD, attenuate NASH and NASH-induced HCC in mice and human NAFLD. In contrast, sulindac did not prevent NASH development in mice, supporting the notion that, rather than the use of NSAIDs in general, more specific APT is required to prevent NASH and NASH-associated conditions.

It is becoming increasingly clear that beyond their central role in hemostasis and wound repair after vascular injury[53], platelets are key players in multiple pathophysiological conditions including thrombosis, atherosclerosis, metastasis and stroke, as well as liver disease. Several studies have demonstrated the role of platelets in viral models of murine hepatitis[21,25,54], human liver regeneration, ischemia-reperfusion injury[55], and bile duct ligation-induced cholestasis[56]. Similarly, results from an *in vivo* rat study supports a role for platelets in fatty liver disease[24]. However, the drug used in this study, cilostizol, has several off-target effects. Here, we show that more specific APT, treatment with a P2Y12 antagonist, depletion of functional GPIbα or lack of α-granules not only abolished activation, accumulation and adhesion of platelets to the liver endothelium but also reduced intrahepatic immune-cell trafficking, consequently reducing liver damage and attenuating disease

development. It has been reported that mean platelet volume (MPV) is increased in NAFLD patients[57], and the MPV is correlated with histological severity of steatosis and fibrosis in NASH[58]. In both, a retrospective and a prospective human cohort study, we demonstrated that APT reduces liver enzymes, liver volume and steatosis in NAFLD patients, supporting the results of our *in vivo* experiments. Interestingly, a cross-sectional analysis suggests that regular aspirin use may be associated with a lower prevalence of NAFLD[59].

A growing body of evidence highlights platelets as active players in liver disease and inflammation[21-23]. Notably, it has been reported that activated platelets contribute to cytotoxic T lymphocyte (CTL)-mediated liver damage and associated pathologies[25]. Moreover, blocking platelet activation and aggregation by Asp-Clo abrogates T cell influx into the liver and subsequent liver damage without affecting peripheral T cell function[26,27]. In our study, deficiencies in GPIIb/IIIa, GPVI or P-selectin were insufficient to abrogate NASH, whereas functional GPIbα deletion or lack of α-granules (*Nbeal2*$^{-/-}$ mice) were sufficient to abolish NASH development. As the knock-out in *Nbeal2*$^{-/-}$ mice is not platelet-specific, other platelet independent co-founding factors cannot be excluded in this model. Strikingly, concomitant with reduced liver damage and NASH, we identified a strong reduction in intrahepatic CD8^{+} T- and NKT cells, granulocytes and myeloid cells in hIL4rα/GP1bα-Tg mice on CD-HFD. Remarkably, functional deficiency of GPIbα alone sufficed to prevent the NASH-associated increase in intrahepatic platelet accumulation.

Confocal analyses and 3D reconstruction revealed that Asp-Clo treatment strongly reduced platelet-immune cell interactions resulting in reduced intrahepatic inflammation. These data confirm that platelets not only become activated in the context of NASH, but also efficiently interact with immune cells and liver endothelial

cells. In this context, intrahepatic platelet adhesion and activation - which depended on GPIbα - facilitate the influx of innate and adaptive immune cells into the liver, thereby exacerbating steatosis, chronic liver damage and NASH. Elucidating the molecular mechanism how activated platelets bind immune cells in NASH warrants further experiments.

In contrast to the central role of GPIbα, we found no evidence for a role of GPIIb/IIIa (*Itga2b*$^{-/-}$ mice) in NASH development, suggesting platelet activation and adhesion to be important and platelet accumulation to be dispensable. Moreover, our results indicate a major contribution of α-granule components to NASH, as shown by the marked protection of *Nbeal2*$^{-/-}$ mice. Importantly, clopidogrel reduces platelet activation and the resulting release of α-granule-stored proteins that are likely involved in platelet-leukocyte-endothelium interactions[60]. The nature of these α-granule constituents is currently still unclear, but our data clearly argue against a major role of P-selectin in this process.

The key role of GPIbα for NASH development identified in this study parallels a similarly vital function of this receptor in the development of experimental autoimmune encephalomyelitis (EAE), in which it orchestrates the recruitment of leukocytes to the inflamed CNS[61]. So far, it is unknown which ligands of GPIbα are relevant for EAE or NASH. However, our results argue against a key role for the two cognate interaction partners of GPIbα, vWF and P-selectin[62,63]. In line, selectins have been shown to be dispensable for leukocyte recruitment into the inflamed liver microvasculature[64].

Other interaction partners might be involved (e.g. Mac-1, or co-agulation factors XI, XII). It is also conceivable that GPIbα exerts its function in disease development independent of a ligand[65]. Moreover, due to the complex pathogenesis underlying

NASH, it is conceivable that GPIbα is not the only molecule involved. The prevention of NASH ultimately suppressed subsequent HCC formation, mostly because the pro-carcinogenic NASH-related environment (e.g. intrahepatic inflammation, hepatocyte damage) was lacking. Thus, our findings provide a rationale for APT, P2Y12 antagonists or reagents directly blocking GPIbα or related pathways as possible therapeutic approaches for NASH.

METHODS

Methods, including statements of data availability and any associated accession codes and references are available in the online version of the paper.

ACKNOWLEDGMENTS

We thank Danijela Heide, Tjeerd Sijmonsma, Jenny Hetzer, Ruth Hillermann, Daniel Kull, Reiner Dunkl, Olga Seelbach, Marion Bawohl, Renaud Maire, Monika Bieri, Christiane Mittmann, Hanna Honcharova-Biletska, André Fitsche, Patrick Münzer, Arlind Adili, Patrick Münzer and Fabiola Prutek for excellent technical assistance. M.M. was partially supported by grants from the University Research Priority Program (URPP) “Integrative Human Physiology”, from the Hartmann Müller Stiftung Zurich. M.H. was supported by an ERC Consolidator grant (HepatoMetaboPath), SFBTR 209 and SFBTR179. This project has received funding from the European Union’s Horizon 2020 research and innovation program under grant agreement No 667273 and the DFG (SFB 688 to B.N., D.S.). ERC Consolidator grant “CholangioConcept” (to L.Z.), the German Research Foundation (DFG): grants FOR2314, SFB685 and the Gottfried Wilhelm Leibniz Program (to L.Z.). Further funding was provided by the German Ministry for Education and Research (BMBF) (eMed/Multiscale HCC), the German Universities Excellence Initiative (third funding line: ‘future concept’), the German Center for Translational Cancer Research (DKTK) and the German-Israeli Cooperation in Cancer Research (DKFZ-MOST) (to L.Z.). D.I. was supported by an EMBO Long-term Fellowship. JML is supported by Asociación Española Contra el Cáncer, Spanish National Health Institute (SAF2013–41027), Generalitat de Catalunya (SGR 1162), Samuel Waxman Cancer Research Foundation, and US Department of Defense (CA150272P3).

AUTHOR CONTRIBUTIONS

Design of the study: M.M., M.J.W., D.R., A.W., B.N., M.G. and M.H. M.M., E.K., D.P., V.L. M.J.W. performed breeding and housing of mice. M.M., E.K., D.P., V.L., D.I., C.D., J.V., D.S., D.D., C.W., P.H., A.R., A.T., P.L. performed experiments. D.R., M.R., F.B., T.G., M.B., M.K. and M.G. designed and performed the clinical trial study. J.W., J.M., R.P., N.D., L.Z., H.A. provided tissue samples or mouse strains and/or scientific input. K.U. performed bio-statistical analyses. All authors analyzed data. M.M., M.E.H., A.W., B.N., M.G. and M.H. wrote the manuscript, and all authors contributed to writing and provided feedback.

COMPETING FINANCIAL INTERESTS

The authors declare no competing financial interests.

FIGURE LEGEND

Figure 1: Increase in platelet numbers and aggregates in liver sinusoids in murine and human NASH. (a) Immunohistochemistry (IHC) for platelets; arrow indicating CD42b+ platelets (n=10 each group). Scale bar: 50 µm. **(b)** Representative 3D confocal micrographs and quantification of hepatic intra-sinusoidal platelets, platelet aggregate size of ND and CD-HFD-fed mice (n=4 mice per group). Sinusoids: gray. Platelets: green. Scale bar: 10 µm. See also Movies S1 and S2. **(c)** Representative and quantitative IHC staining of $CD42b^+$ intra-sinusoidal platelets in hURI-tetOFF^{hep} mice, a mouse model of NASH (n=6 per each group). Scale bar: 50µm. **(d)** IHC and quantification of platelets (CD61) in human livers with NASH or without liver disease. Arrows indicate intra-sinusoidal platelets (non-diseased n=4; NASH patients n=18). **(e)** IHC and quantification for $CD42b^+$ platelets in ND, CD-HFD and CD-HFD/Asp-Clo treated C57BL/6 mice of paraffin-embedded liver sections. ND, CD-HFD group are the identical cohorts used in **a**. Asp-Clo (n=10). **(f)** AST and ALT level of a retrospective analysis of patients before study inclusion and after 6 months of anti-platelet therapy (APT) (n=148). **(g)** Magnetic resonance imaging / ultrasound of the abdomen of representative patients included into a prospective trial before study inclusion and after 6 months of APT (n=18). **(h)** Liver fat, liver mass and liver damage were quantified and blotted. All data are shown as mean ± SEM.*: $P < 0.05$. **: $P < 0.01$. ***: $P < 0.001$. ****: $P < 0.0001$. N.s.: Not significant.

Figure 2: Asp-Clo as anti-platelet treatment results in reduction of steatosis, liver damage, NASH and NASH-associated conditions. (a) Body weights monitored for ND, CD-HFD and CD-HFD/Asp-Clo-fed C57BL/6 mice (n=10 per each group) over 12 months. Black asterisks: comparison of ND with CD-HFD. Green asterisks: comparison of ND with CD-HFD/Asp-Clo C57BL/6 mice. **(b)** Quantification of serum ALT in ND, CD-HFD and CD-HFD/Asp-Clo fed C57BL/6 mice (n≥7 per each group). **(c)** IPGTT performed with 6-month-old ND, CD-HFD and CD-HFD/Asp-Clo C57BL/6 mice (n=5 per each group). Black asterisks: Comparison of ND and CD-HFD. Green asterisks: Comparison CD-HFD with CD-HFD/Asp-Clo. **(d)** Liver triglyceride analysis in 6 and 12-month-old ND, CD-HFD and CD-HFD/Asp-Clo fed C57BL/6 mice (n ≥7 per each group). **(e)** Quantification of serum cholesterol in ND, CD-HFD and CD-HFD/Asp-Clo-fed C57BL/6 mice at 6 and 12 month time-points (n≥7 per each group). **(f)** Real-time PCR analysis for hepatic mRNA expression of genes involved in lipid metabolism/β-oxidation in ND (n=4), CD-HFD (n=5) and CD-HFD/Asp-Clo-fed (n=7) C57BL/6 livers. Green stars: comparison of CD-HFD with CD-HFD/Asp-Clo. **(g)** MRI analyses on livers of 6-month-old ND, CD-HFD and Cd-HFD/Asp-Clo fed C57BL/6 mice. T1 (fast low-

angle shot [FLASH]) OUT phase: dark colour indicative of steatosis. T2 TurboRare visualizes increase in subcutaneous and abdominal fat and hepatic lipid accumulation (bright regions) in CD-HFD and CD-HFD/Asp-Clo mice. **(h)** Liver histology of ND, CD-HFD and CD-HFD/Asp-Clo-fed C57BL/6 mice stained with H/E. Scale bar represents 100µm in 10X, 50µm in 20X and 25µm in 40X. **(i)** Sudan red staining of liver sections indicating fact accumulation in ND, CD-HFD and CD-HFD/Asp-Clo fed C57BL/6 mice. Scale bar: 100µm. (n≥4 mice for each group). All data are shown as mean ± SEM.*: P < 0.05. **: P < 0.01. ***: P < 0.001. ****: P < 0.0001. N.s.: Not significant.

Figure 3: Anti-platelet treatment with Asp-Clo abrogates immune cells infiltration into the liver and prevents NASH-induced HCC development. (a) Histology (H/E) and IHC [$B220^+$ (B cells), $CD3^+$ (T cells), $F4/80^+$ (Kupffer cells), $MHCII^+$ (antigen presenting cells e.g. meloid cells) and $Ly\text{-}6G^+$ (granulocytes)] of livers of 6-month-old ND (upper row) and CD-HFD (middle row) and CD-HFD/Asp-Clo-fed (lower row) C57BL/6 mice. The scale bar in H/E represents 100µm, and 50µm in B220, CD3, F4/80, MHCII and Ly-6G staining. **(b)** Representative FACS plot and quantification of whole liver homogenates on 6-month old ND (n=6), CD-HFD (n=6) and CD-HFD/Asp-Clo (n=4) mice. $CD8^+$ and $CD4^-$ (upper panel) and $CD8^+$ $CD44^+$ $CD69^+$ (lower panel). **(c)** Representative Western blot images of the indicated proteins in liver homogenates from ND, CD-HFD and CD-HFD/Asp-Clo-fed C57BL/6 mice. kDa: kilo Dalton. **(d)** Representative macroscopical analysis of livers from 12-month-old ND, CD-HFD and CD-HFD/Asp-Clo-fed C57BL/6 mice. White arrow head: HCC. Scale bar: 7.5 mm. **(e)** Quantification of the NASH-induced HCC development (T=HCC excluding adenoma; NT=non-tumor). This graph presents the CD-HFD/Asp-Clop treatment with weight adjusted dose (ND n=17; CD-HFD n=51 and CD-HFD/Asp-Clo n=20). Each symbol represents an individual mouse. HCC incidence was calculated using Fisher's exact test. **(f)** Liver histology and IHC of 12-month-old C57BL/6 mice on ND (upper row) and CD-HFD with HCC (middle row) and CD-HFD/Asp-Clo (lower row). Col IV: Collagen IV. Dashed line depicts HCC border. Scale bars: 2 mm (low; H/E) and 200 µm (high; H/E; Col IV). All data are shown as mean ± SEM.*: P < 0.05. **: P < 0.01. ***: P < 0.001. ****: P < 0.0001. N.s.: Not significant.

Figure 4: Ticagrelor treatment attenuates CD-HFD-induced NASH, NASH-associated conditions and prevents HCC. (a) Body weight monitored for ND, CD-HFD and CD-HFD/ticagrelor-fed C57BL/6 mice (n≥5 for each group) over 12 months. Black asterisks: comparison of ND and CD-HFD Green asterisks: comparison of CD-HFD with CD-HFD/ticagrelor. **(b)** Quantification of serum ALT levels in 6-month-old ND, CD-HFD and CD-

HFD/ticagrelor-fed C57BL/6 mice (n≥5 for each group). **(c)** Liver triglyceride content of 6-month old ND, CD-HFD and CD-HFD/ticagrelor fed C57BL/6 mice (n≥5 for each group). **(d)** Quantification of serum cholesterol over 6 months in ND, CD-HFD and CD-HFD/ticagrelor fed mice (n≥5 for each group). **(e)** Liver histology from 6-month-old ND, CD-HFD and CD-HFD/ticagrelor fed C57BL/6 mice. Ballooned hepatocytes (asterisk) and satellitosis (arrow) are indicated. **(f)** Sudan red staining and quantification for fat accumulation/macrovesicular steatosis in livers of ND, CD-HFD and CD-HFD/ticagrelor-fed C57BL/6 mice. Scale bar: 100µm. **(g)** FACS analysis of whole liver of 6-month-old ND, CD-HFD and CD-HFD/Asp-Clo-fed C57Bl/6 mice (n≥4 mice per each group). $CD8^+CD4^-$ (upper panel) and $CD8^+CD62L^-D44^+CD69^+$ (lower panel) are shown. **(h)** Absolute quantification of intrahepatic $CD8^+$ and $CD4^-$ and $CD8^+$ $CD44^+$ $CD69^+$ cells in 6-month-old ND, CD-HFD and CD-HFD/Asp-Clo-fed C57Bl/6 mice. **(i)** IHC of $CD3^+$, $F480^+$ and $MHCII^+$ cells in liver sections of 6-month-old ND, CD-HFD and CD-HFD/Asp-Clo fed C57Bl/6 mice. **(j)** Macroscopic analysis of livers at 12 months of age. White arrow head: HCC. **(k)** NASH-induced HCC development (T=HCC and NT=non tumor, (ND n=17; CD-HFD n=51 and CD-HFD/Asp-Clo n=20) was analysed and quantified. ND and CD-HFD groups are shared with Figure 3e. All data are shown as mean ± SEM.*: P < 0.05. **: P < 0.01. ***: P < 0.001. ****: P < 0.0001. N.s.: Not significant.

Figure 5: GPIbα and α-granules, but not platelet aggregation are critical for development of steatosis, NASH and NASH-associated conditions. (a) IHC for $CD42b^+$ platelets (arrow) in livers of CD-HFD fed mice treated with GPIbα blocking Fab or control antibody injected into CD-HFD fed mice (n≥3 mice per group). $CD42b^+$ platelets were quantified per 139mm^2. **(b)** Body weight gain in ND, CD-HFD and CD-HFD/hIL4rα/GP1bα-Tg C57BL/6 mice over 6 months. Black asterisks: comparison of ND and CD-HFD. Blue asterisks: comparison of CD-HFD and CD-HFD/hIL4rα/GP1bα-Tg mice (n≥4 for each group). **(c)** Serum ALT levels, **(d)** liver triglyceride, **(e)** serum cholesterol, **(f)** serum LDL and **(g)** serum HDL in ND, CD-HFD C57Bl/6 and CD-HFD/hIL4rα/GP1bα-Tg C57BL/6 mice (n≥4 for each group). **(h)** Real-time PCR analysis for mRNA expression of genes involved in lipid metabolism/b-oxidation from livers of ND, CD-HFD C57Bl/6 and CD-HFD/GP1bα-IL4r-Tg mice (ND n=4; CD-HFD n=4; CD-HFD/hIL4rα/GP1bα-Tg n=3). Green asterisk: comparison of CD-HFD with CD-HFD/hIL4rα/GP1bα-Tg C57BL/6 mice. **(i)** Liver histology (H/E) of CD-HFD and CD-HFD-fed hIL4rα/GP1bα-Tg mice. Histological features of NASH are indicated: ballooned hepatocytes (asterisks); satellitosis (arrows). Scale bars: 100 µm in 10X, 50 µm in 20X and 25 µm in 40X. **(j)** Sudan red staining and quantification for accumulation of fat and macrovesicular steatosis in livers of 6-month-old ND, CD-HFD C57Bl/6 and CD-HFD/hIL4rα/GP1bα-Tg mice (n≥5 for each group). Scale bar: 100 µm. **(k)** Body weight

development was monitored for ND, CD-HFD C57Bl/6 and CD-HFD/*Itga2b*$^{-/-}$ mice over 6 months. Black asterisks indicate the comparison between ND and CD-HFD C57Bl/6 mice. Dark blue asterisks indicate a comparison between ND C57Bl/6 and CD-HFD/*Itga2b*$^{-/-}$ mice. **(l)** Liver/body weight ratio in the ND, CD-HFD C57Bl/6 and CD-HFD-fed *Itga2b*$^{-/-}$ mice at 6 months. **(m)** Serum ALT and AST levels, **(n)** liver triglycerides, **(o)** serum cholesterol and **(p)** Sudan red staining of livers from the indicated groups at the 6 month time-point (ND n=5; CD-HFD n=5; CD-HFD/Itga2b$^{-/-}$ n=4). Scale bar: 50μm. All data are shown as mean ± SEM.*: P < 0.05. **: P < 0.01. ***: P < 0.001. ****: P < 0.0001. N.s.: Not significant.

Figure 6: Asp-Clo treatment reduces platelet activation/aggregation, cytokine release and platelet/liver endothelium and platelet/immune-cell interaction. (a) GESA of the most important significantly changed hepatic gene clusters representing transcriptional changes in platelet related gene expression, positive regulation of TNF-superfamily members, cytokine expression/cytokine/receptors interaction and immune-cell attraction in livers of ND- vs. CD-HFD-fed mice. **(b)** Analysis of chemokines and cytokines in whole liver extracts by multiplex ELISA. Normalized amount of liver protein extracts were analyzed in ND, CD-HFD and Asp-Clo treated CD-HFD fed mice (data are pooled from two independent experiments, n≥10 per each group). **(c)** Representative 3D confocal micrographs and quantification of the platelet/liver endothelium interaction in the liver of ND, CD-HFD, CD-HFD/Asp-Clo, CD-HFD/ticagrelor C57Bl/6 and CD-HFD/hIL4rα/GP1bα-Tg mice (n=4 mice per group) are shown. Sinusoids are presented in gray, platelets in green. Scale bar: 20 μm. **(d)** Quantification of platelet aggregate size, overall platelet (PLT) surface and quantification of platelet/liver endothelium coverage are shown in focus of view (FOV; n=4 mice per group). For visualization of intravascular events and to increase image clarity, the transparency of the sinusoidal rendering was set to 50%. **(e)** 3D confocal images from livers of ND, CD-HFD fed mice and also Asp-Clo treated CD-HFD fed mice for platelet (green)/CD3$^+$ T cells (red) interaction in the identical mice visualized for (c). Sinusoids are presented in gray. Scale bar represents 20 μm. Platelet/CD3$^+$ T interaction count and platelet/CD3$^+$ T cell interaction (in %) are quantified. FOV: focus of view (the same mice used for (d). **(f)** Histograms of CD3$^+$ T (red) and endothelial cells (gray) underlining increased CD3$^+$ T cells/liver endothelium. **(g)** 3D confocal images from livers of ND, CD-HFD and CD-HFD/Asp-Clo treated CD-HFD mice for platelets (green)/CD11b$^+$ myeloid cells (red) interaction in the identical mice visualized for (c). Sinusoids are presented in gray. Scale bar represents 20 μm. Platelet/CD11b$^+$ interactions are quantified. All data are shown as mean ± SEM.*: P < 0.05. **: P < 0.01. ***: P < 0.001. ****: P < 0.0001. N.s.: Not significant.

References

1. El-Serag, H.B. & Kanwal, F. Epidemiology of hepatocellular carcinoma in the United States: where are we? Where do we go? *Hepatology* **60**, 1767-1775 (2014).
2. Torre, L.A.*, et al.* Global cancer statistics, 2012. *CA: a cancer journal for clinicians* **65**, 87-108 (2015).
3. http://www.who.int. Cancer (2017).
4. Fleet, S.E., Lefkowitch, J.H. & Lavine, J.E. Current Concepts in Pediatric Nonalcoholic Fatty Liver Disease. *Gastroenterol Clin North Am* **46**, 217-231 (2017).
5. European Association for the Study of the, L., European Association for the Study of, D. & European Association for the Study of, O. EASL-EASD-EASO Clinical Practice Guidelines for the management of non-alcoholic fatty liver disease. *J Hepatol* **64**, 1388-1402 (2016).
6. Charlton, M.R.*, et al.* Frequency and outcomes of liver transplantation for nonalcoholic steatohepatitis in the United States. *Gastroenterology* **141**, 1249-1253 (2011).
7. Anstee, Q.M. & Day, C.P. The genetics of NAFLD. *Nature reviews. Gastroenterology & hepatology* **10**, 645-655 (2013).
8. Michelotti, G.A., Machado, M.V. & Diehl, A.M. NAFLD, NASH and liver cancer. *Nature reviews. Gastroenterology & hepatology* **10**, 656-665 (2013).
9. Singal, A.G. & El-Serag, H.B. Hepatocellular Carcinoma From Epidemiology to Prevention: Translating Knowledge into Practice. *Clin Gastroenterol Hepatol* **13**, 2140-2151 (2015).
10. Brunt, E.M.*, et al.* Nonalcoholic fatty liver disease. *Nat Rev Dis Primers* **1**, 15080 (2015).
11. Younossi, Z.M.*, et al.* Changes in the prevalence of the most common causes of chronic liver diseases in the United States from 1988 to 2008. *Clin Gastroenterol Hepatol* **9**, 524-530 e521; quiz e560 (2011).
12. Smith, B.W. & Adams, L.A. Nonalcoholic fatty liver disease and diabetes mellitus: pathogenesis and treatment. *Nat Rev Endocrinol* **7**, 456-465 (2011).
13. Perumpail, R.B., Wong, R.J., Ahmed, A. & Harrison, S.A. Hepatocellular Carcinoma in the Setting of Non-cirrhotic Nonalcoholic Fatty Liver Disease and the Metabolic Syndrome: US Experience. *Dig Dis Sci* **60**, 3142-3148 (2015).
14. Collaborators, G.B.D.O.*, et al.* Health Effects of Overweight and Obesity in 195 Countries over 25 Years. *The New England journal of medicine* **377**, 13-27 (2017).
15. Wolf, M.J.*, et al.* Metabolic activation of intrahepatic CD8+ T cells and NKT cells causes nonalcoholic steatohepatitis and liver cancer via cross-talk with hepatocytes. *Cancer cell* **26**, 549-564 (2014).
16. Michelson, A.D. How platelets work: platelet function and dysfunction. *J Thromb Thrombolysis* **16**, 7-12 (2003).
17. Jackson, S.P. Arterial thrombosis--insidious, unpredictable and deadly. *Nature medicine* **17**, 1423-1436 (2011).
18. Huo, Y.*, et al.* Circulating activated platelets exacerbate atherosclerosis in mice deficient in apolipoprotein E. *Nature medicine* **9**, 61-67 (2003).
19. Labelle, M., Begum, S. & Hynes, R.O. Platelets guide the formation of early metastatic niches. *Proceedings of the National Academy of Sciences of the United States of America* **111**, E3053-3061 (2014).
20. Nieswandt, B., Kleinschnitz, C. & Stoll, G. Ischaemic stroke: a thrombo-inflammatory disease? *J Physiol* **589**, 4115-4123 (2011).
21. Lang, P.A.*, et al.* Aggravation of viral hepatitis by platelet-derived serotonin. *Nature medicine* **14**, 756-761 (2008).
22. Ripoche, J. Blood platelets and inflammation: their relationship with liver and digestive diseases. *Clin Res Hepatol Gastroenterol* **35**, 353-357 (2011).
23. Chauhan, A., Adams, D.H., Watson, S.P. & Lalor, P.F. Platelets: No longer bystanders in liver disease. *Hepatology* **64**, 1774-1784 (2016).

24. Fujita, K.*, et al.* Effectiveness of antiplatelet drugs against experimental non-alcoholic fatty liver disease. *Gut* **57**, 1583-1591 (2008).
25. Iannacone, M.*, et al.* Platelets mediate cytotoxic T lymphocyte-induced liver damage. *Nature medicine* **11**, 1167-1169 (2005).
26. Iannacone, M., Sitia, G., Narvaiza, I., Ruggeri, Z.M. & Guidotti, L.G. Antiplatelet drug therapy moderates immune-mediated liver disease and inhibits viral clearance in mice infected with a replication-deficient adenovirus. *Clin Vaccine Immunol* **14**, 1532-1535 (2007).
27. Sitia, G.*, et al.* Antiplatelet therapy prevents hepatocellular carcinoma and improves survival in a mouse model of chronic hepatitis B. *Proceedings of the National Academy of Sciences of the United States of America* **109**, E2165-2172 (2012).
28. Musso, G., Cassader, M., Rosina, F. & Gambino, R. Impact of current treatments on liver disease, glucose metabolism and cardiovascular risk in non-alcoholic fatty liver disease (NAFLD): a systematic review and meta-analysis of randomised trials. *Diabetologia* **55**, 885-904 (2012).
29. Wong, V.W.*, et al.* Pathogenesis and novel treatment options for non-alcoholic steatohepatitis. *Lancet Gastroenterol Hepatol* **1**, 56-67 (2016).
30. Gomes, A.L.*, et al.* Metabolic Inflammation-Associated IL-17A Causes Non-alcoholic Steatohepatitis and Hepatocellular Carcinoma. *Cancer cell* **30**, 161-175 (2016).
31. Mauri, L.*, et al.* Twelve or 30 months of dual antiplatelet therapy after drug-eluting stents. *The New England journal of medicine* **371**, 2155-2166 (2014).
32. He, G.*, et al.* Hepatocyte IKKbeta/NF-kappaB inhibits tumor promotion and progression by preventing oxidative stress-driven STAT3 activation. *Cancer cell* **17**, 286-297 (2010).
33. He, G. & Karin, M. NF-kappaB and STAT3 - key players in liver inflammation and cancer. *Cell Res* **21**, 159-168 (2011).
34. Thun, M.J., Jacobs, E.J. & Patrono, C. The role of aspirin in cancer prevention. *Nat Rev Clin Oncol* **9**, 259-267 (2012).
35. Husted, S. & van Giezen, J.J. Ticagrelor: the first reversibly binding oral P2Y12 receptor antagonist. *Cardiovasc Ther* **27**, 259-274 (2009).
36. Anderson, S.D., Shah, N.K., Yim, J. & Epstein, B.J. Efficacy and safety of ticagrelor: a reversible P2Y12 receptor antagonist. *Ann Pharmacother* **44**, 524-537 (2010).
37. Kunishima, S., Kamiya, T. & Saito, H. Genetic abnormalities of Bernard-Soulier syndrome. *Int J Hematol* **76**, 319-327 (2002).
38. Blenner, M.A., Dong, X. & Springer, T.A. Structural basis of regulation of von Willebrand factor binding to glycoprotein Ib. *J Biol Chem* **289**, 5565-5579 (2014).
39. Kleinschnitz, C.*, et al.* Targeting platelets in acute experimental stroke: impact of glycoprotein Ib, VI, and IIb/IIIa blockade on infarct size, functional outcome, and intracranial bleeding. *Circulation* **115**, 2323-2330 (2007).
40. Kanaji, T., Russell, S. & Ware, J. Amelioration of the macrothrombocytopenia associated with the murine Bernard-Soulier syndrome. *Blood* **100**, 2102-2107 (2002).
41. Sadler, J.E. Biochemistry and genetics of von Willebrand factor. *Annu Rev Biochem* **67**, 395-424 (1998).
42. Auton, M., Zhu, C. & Cruz, M.A. The mechanism of VWF-mediated platelet GPIbalpha binding. *Biophys J* **99**, 1192-1201 (2010).
43. Jandrot-Perrus, M.*, et al.* Cloning, characterization, and functional studies of human and mouse glycoprotein VI: a platelet-specific collagen receptor from the immunoglobulin superfamily. *Blood* **96**, 1798-1807 (2000).
44. Deppermann, C.*, et al.* Gray platelet syndrome and defective thrombo-inflammation in Nbeal2-deficient mice. *J Clin Invest* (2013).
45. Albers, C.A.*, et al.* Exome sequencing identifies NBEAL2 as the causative gene for gray platelet syndrome. *Nat Genet* **43**, 735-737 (2011).
46. Kahr, W.H.*, et al.* Mutations in NBEAL2, encoding a BEACH protein, cause gray platelet syndrome. *Nat Genet* **43**, 738-740 (2011).

47. Gunay-Aygun, M*., et al.* NBEAL2 is mutated in gray platelet syndrome and is required for biogenesis of platelet alpha-granules. *Nat Genet* **43**, 732-734 (2011).
48. Subramaniam, M*., et al.* Defects in hemostasis in P-selectin-deficient mice. *Blood* **87**, 1238-1242 (1996).
49. Kral, J.B., Schrottmaier, W.C., Salzmann, M. & Assinger, A. Platelet Interaction with Innate Immune Cells. *Transfus Med Hemother* **43**, 78-88 (2016).
50. Townsend, S.A. & Newsome, P.N. Non-alcoholic fatty liver disease in 2016. *Br Med Bull* **119**, 143-156 (2016).
51. Neuschwander-Tetri, B.A*., et al.* Farnesoid X nuclear receptor ligand obeticholic acid for non-cirrhotic, non-alcoholic steatohepatitis (FLINT): a multicentre, randomised, placebo-controlled trial. *Lancet* **385**, 956-965 (2015).
52. Franchi, F., Rollini, F. & Angiolillo, D.J. Antithrombotic therapy for patients with STEMI undergoing primary PCI. *Nat Rev Cardiol* **14**, 361-379 (2017).
53. George, J.N. Platelets. *Lancet* **355**, 1531-1539 (2000).
54. Sitia, G., Iannacone, M. & Guidotti, L.G. Anti-platelet therapy in the prevention of hepatitis B virus-associated hepatocellular carcinoma. *J Hepatol* **59**, 1135-1138 (2013).
55. Lesurtel, M*., et al.* Platelet-derived serotonin mediates liver regeneration. *Science* **312**, 104-107 (2006).
56. Laschke, M.W., Dold, S., Menger, M.D., Jeppsson, B. & Thorlacius, H. Platelet-dependent accumulation of leukocytes in sinusoids mediates hepatocellular damage in bile duct ligation-induced cholestasis. *Br J Pharmacol* **153**, 148-156 (2008).
57. Ozhan, H*., et al.* Mean platelet volume in patients with non-alcoholic fatty liver disease. *Platelets* **21**, 29-32 (2010).
58. Alkhouri, N*., et al.* Mean platelet volume as a marker of increased cardiovascular risk in patients with nonalcoholic steatohepatitis. *Hepatology* **55**, 331 (2012).
59. Shen, H., Shahzad, G., Jawairia, M., Bostick, R.M. & Mustacchia, P. Association between aspirin use and the prevalence of nonalcoholic fatty liver disease: a cross-sectional study from the Third National Health and Nutrition Examination Survey. *Aliment Pharmacol Ther* **40**, 1066-1073 (2014).
60. Smyth, S.S*., et al.* Beta(3)-integrin-deficient mice but not P-selectin-deficient mice develop intimal hyperplasia after vascular injury: correlation with leukocyte recruitment to adherent platelets 1 hour after injury. *Circulation* **103**, 2501-2507 (2001).
61. Langer, H.F*., et al.* Platelets contribute to the pathogenesis of experimental autoimmune encephalomyelitis. *Circ Res* **110**, 1202-1210 (2012).
62. Romo, G.M*., et al.* The glycoprotein Ib-IX-V complex is a platelet counterreceptor for P-selectin. *J Exp Med* **190**, 803-814 (1999).
63. Kroll, M.H., Harris, T.S., Moake, J.L., Handin, R.I. & Schafer, A.I. von Willebrand factor binding to platelet GpIb initiates signals for platelet activation. *J Clin Invest* **88**, 1568-1573 (1991).
64. Wong, J*., et al.* A minimal role for selectins in the recruitment of leukocytes into the inflamed liver microvasculature. *J Clin Invest* **99**, 2782-2790 (1997).
65. Dutting, S*., et al.* A Cdc42/RhoA regulatory circuit downstream of glycoprotein Ib guides transendothelial platelet biogenesis. *Nat Commun* **8**, 15838 (2017).

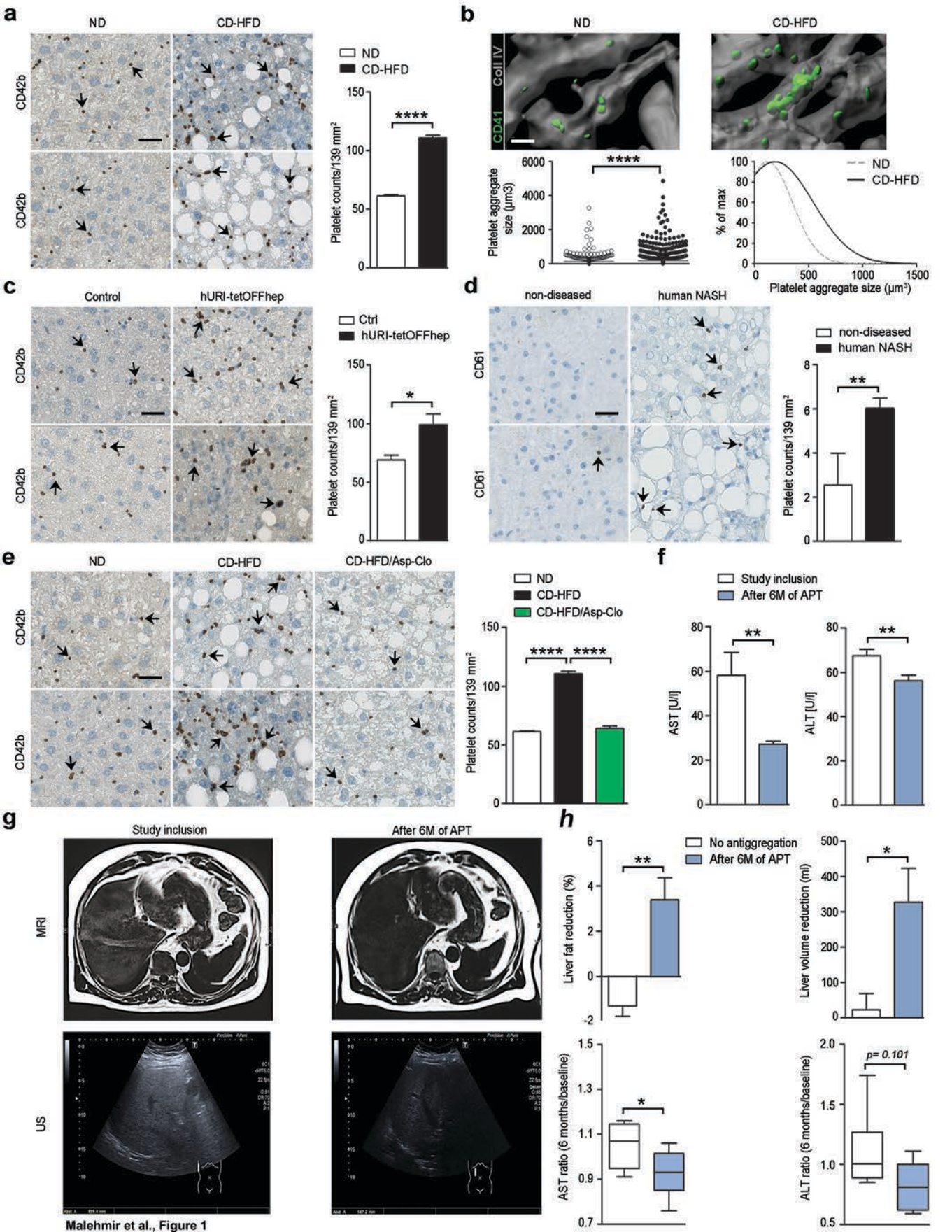

Malehmir et al., Figure 1

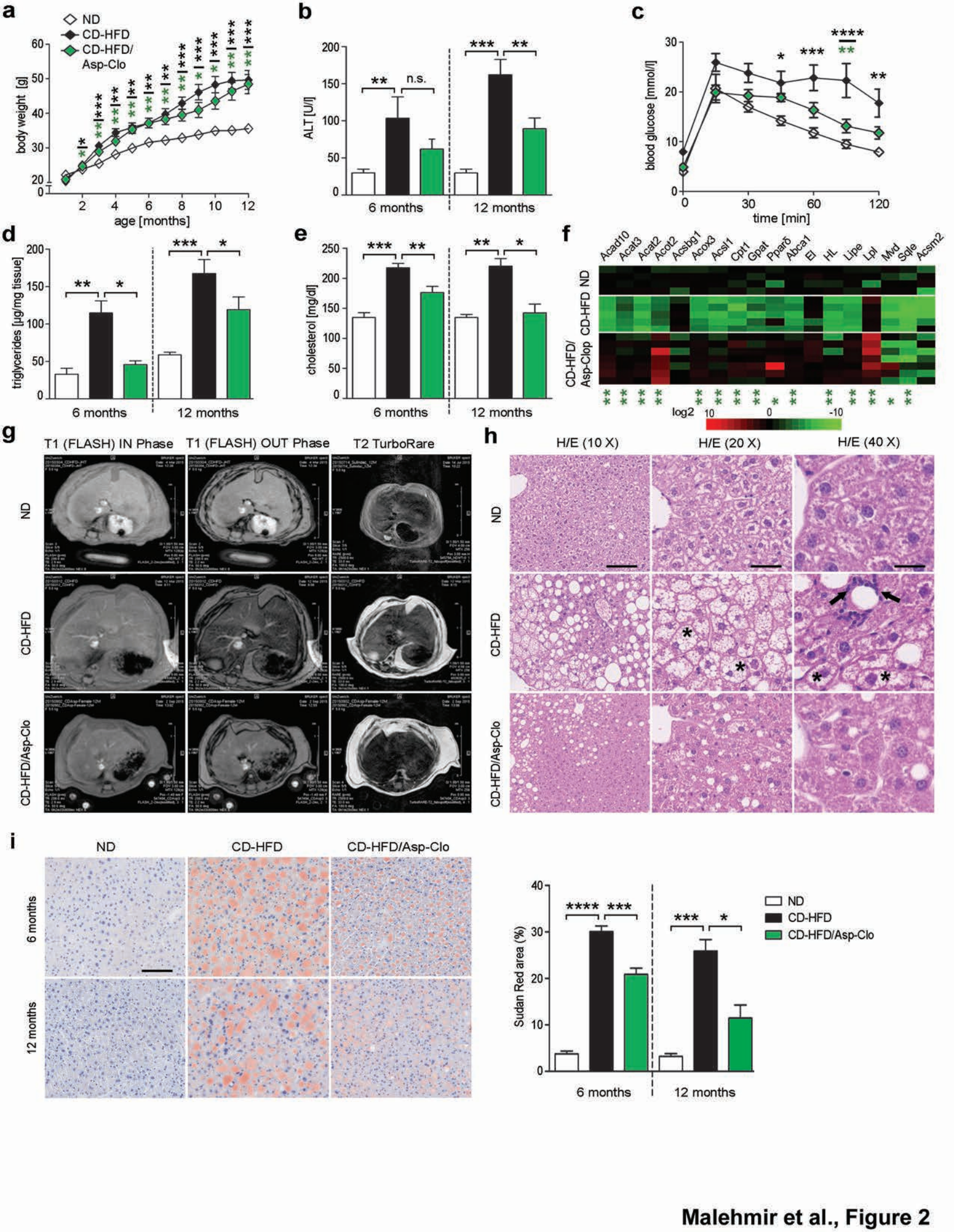

Malehmir et al., Figure 2

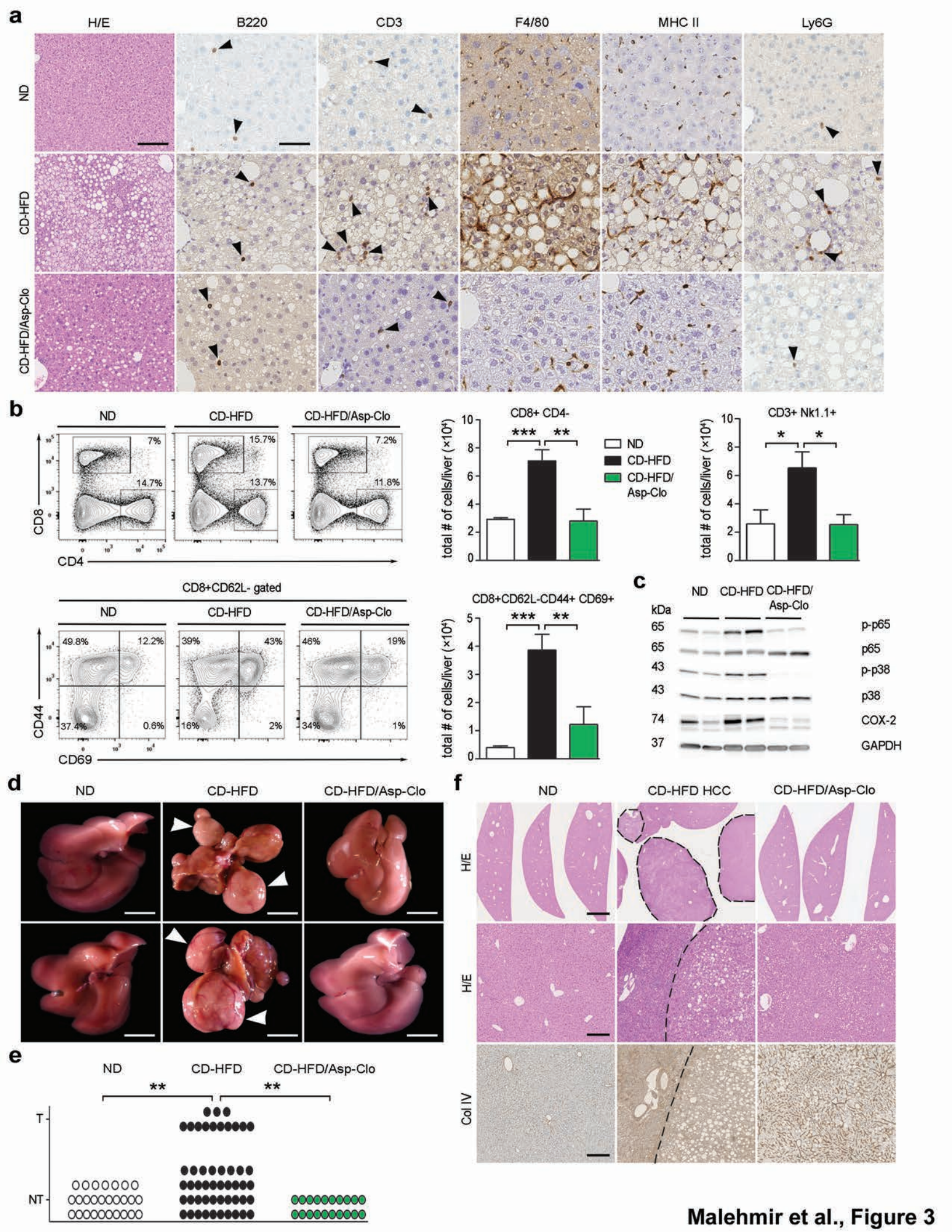

Malehmir et al., Figure 3

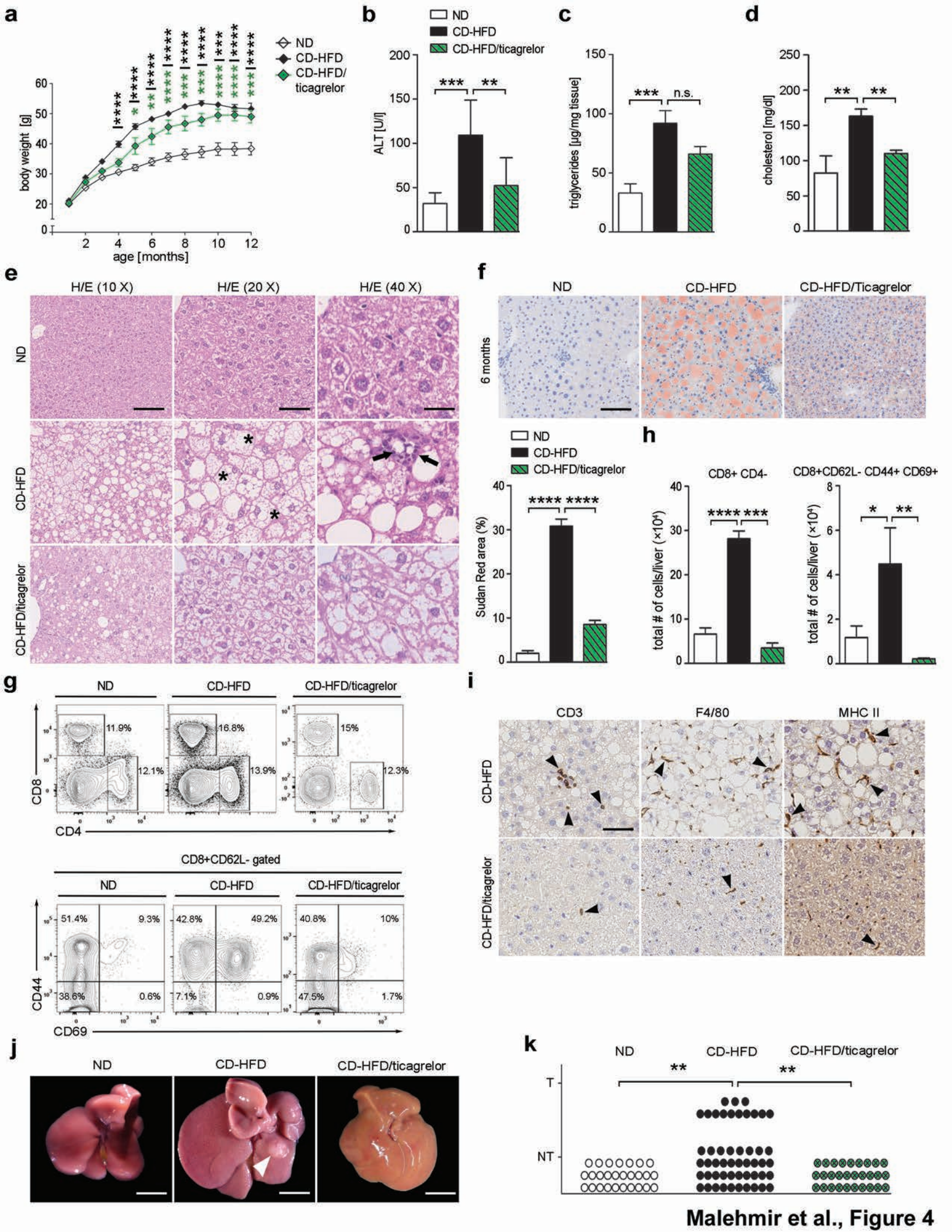
a
ND
CD-HFD
CD-HFD/ ticagrelor
body weight [g]
age [months]
b
ALT [U/l]
c
triglycerides [µg/mg tissue]
n.s.
d
cholesterol [mg/dl]
e
H/E (10 X)
H/E (20 X)
H/E (40 X)
CD-HFD/ticagrelor
f
ND
CD-HFD
CD-HFD/Ticagrelor
6 months
Sudan Red area (%)
h
CD8+ CD4-
CD8+CD62L- CD44+ CD69+
total # of cells/liver (×10⁴)
g
11.9%
12.1%
16.8%
13.9%
15%
12.3%
CD8
CD4
CD8+CD62L- gated
51.4%
9.3%
38.6%
0.6%
42.8%
49.2%
7.1%
0.9%
40.8%
10%
47.5%
1.7%
CD44
CD69
i
CD3
F4/80
MHC II
j
k
T
NT
Malehmir et al., Figure 4

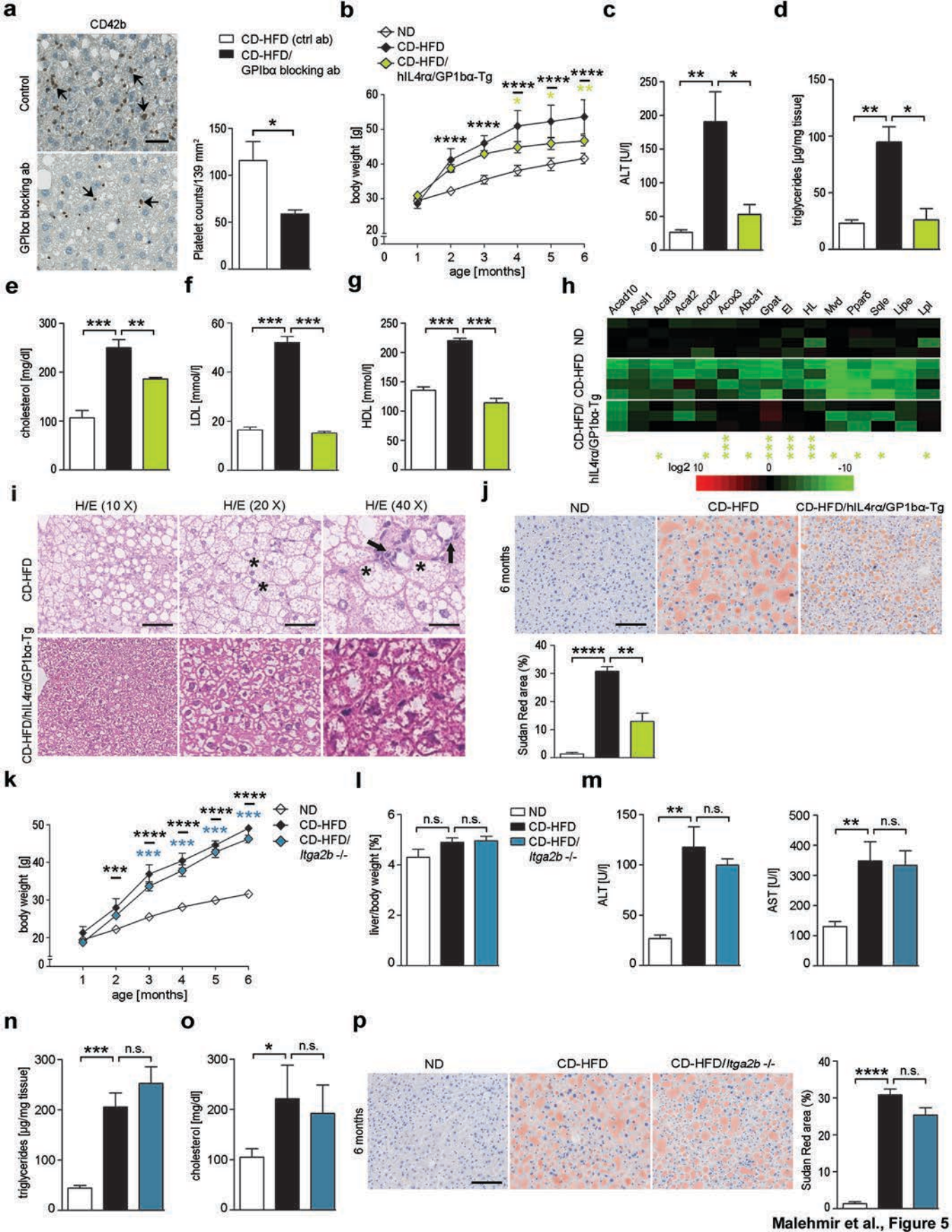

Malehmir et al., Figure 5

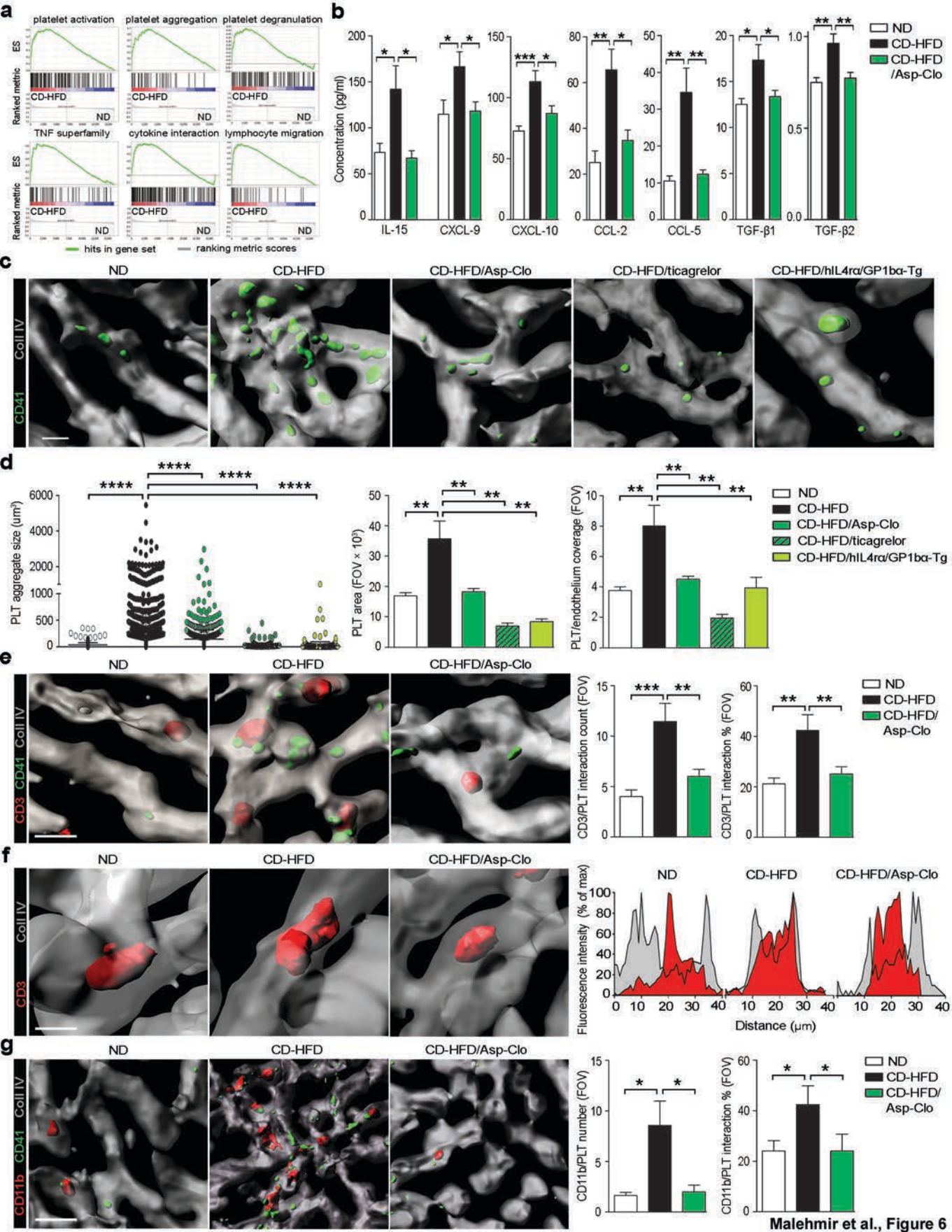

Malehmir et al., Figure 6